RAPID COMMUNICATION

Nano-infrared imaging of localized plasmons in graphene nano-resonators*

Jiahua Duan(段嘉华)[1,2], Runkun Chen(陈闰堃)[1,2], and Jianing Chen(陈佳宁)[1,2,3,†]

[1] *Beijing National Laboratory for Condensed Matter Physics, Institute of Physics, Chinese Academy of Sciences, Beijing* 100190, *China*
[2] *School of Physical Sciences, University of Chinese Academy of Sciences, Beijing* 100049, *China*
[3] *Collaborative Innovation Center of Quantum Matter, Beijing* 100190, *China*

(Received 11 August 2017; revised manuscript received 31 August 2017; published online 30 September 2017)

We conduct *in-situ* near-field imaging of propagating and localized plasmons (cavity and dipole modes) in graphene nano-resonator. Compared with propagating graphene plasmons, the localized modes show twofold near-field amplitude and high volume confining ability ($\sim 10^6$). The cavity resonance and dipole mode of graphene plasmons can be effectively controlled through optical method. Furthermore, our numerical simulation shows quantitative agreement with experimental measurements. The results provide insights into the nature of localized graphene plasmons and demonstrate a new way to study the localization of polaritons in Van der Waals materials.

Keywords: graphene plasmons, nano-resonator, dipole, near-field imaging

PACS: 78.67.Wj, 07.79.Fc, 73.20.Mf **DOI:** 10.1088/1674-1056/26/11/117802

1. Introduction

The conventional Abbe diffraction limit and weak light-matter interaction restrict the nanoscale manipulation of photons, which is the ultimate target of nano-photonics.[1,2] Until now, the most feasible solution to these problems is producing collective excitations named polaritons,[3,4] coupling photons with other easily controlled particles, such as electrons[5,6] or phonons.[7,8] It has been confirmed that polaritons can confine free-space light to nanoscale[9] (λ_0/λ_p up to 150) and enhance the light–matter interaction[10] (such as single-molecule spectrum). Among various kinds of polaritons, the plasmons become one of the most important members due to its ability to merge the photonics and electronics at nanoscale dimensions. Metals with high charge-carrier concentration are the first-generation plasmonic material and play important roles in enhanced spectroscopy,[10,11] quantum circuits,[12,13] photovoltaic devices,[14] nanofocusing,[15,16] etc. However, the problems of absorption losses[17] constrain the operating frequencies of metallic plasmons to visible and near-infrared range. Meanwhile, the charge carrier in noble metals has slow mobility and low Fermi velocity, making plasmons become high loss and un-tunable.

In the ongoing search for better plasmonic media, the two-dimensional materials, or called Van der Waals materials,[18] are found to be a very promising candidate from mid-infrared to terahertz electromagnetic band, filling the gap of metallic plasmons. Due to its unique linear energy dispersion.[20] (Dirac cone) and universal optical conductivity[21,22] ($e^2/4\hbar$), graphene become the most popular plasmonic member[19] among various Van der Waals materials. Compared with conventional metal plasmonics, graphene plasmons provide three advantages. First, graphene is a semimetal, whose carrier concentration is less than ~ 0.01 per atom compared with the case of ~ 1 in gold. That is to say, its plasmonic Drude weight can be effectively tuned by electrical,[23] chemical,[24] or optical[25] approach. Second, the two-dimensional nature of graphene makes its plasmons can be easily tuned[26] through avoiding the usual Coulomb Screening effect. Third, graphene possesses very high charge carrier mobility[27] ascribed to its low density of states and relatively weak electron-phonon interaction. These advantages constitute state-of-the-art graphene plasmonics. Recently, one emerging near-field technique called scattering-type scanning near-field optical microscopy (s-SNOM) directly observed propagating graphene plasmons and reveal its gate-tunable dispersion.[28,29] However, previous reports mainly paid attention to the propagating mode of graphene plasmons and did not give unambiguous demonstration about localized mode, which has higher nano-confining capability and stronger light–matter interaction.

In this paper, we directly observe the *in-situ* transition from propagating to localized plasmons in graphene stripe with continuously changing width from 400 nm ($W_{Gra} \gg \lambda_p$) to 20 nm ($W_{Gra} \ll \lambda_p$). The nano-infrared images reveal that

*Project supported by the National Key Research and Development Program of China (Grant No. 2016YFA0203500), the National Natural Science Foundation of China (Grant No. 11474350), the State Key Laboratory of Optoelectronic Materials and Technologies, Sun Yat-Sen University, China and the State Key Laboratory for Artificial Microstructure & Mesoscopic Physics, Peking University, China.

†Corresponding author. E-mail: jnchen@iphy.ac.cn

© 2017 Chinese Physical Society and IOP Publishing Ltd

there are two kinds of localization, which are cavity mode and dipole mode, respectively. The observed cavity mode possesses higher near-field amplitude ($\sim$ twofold) and three-dimensional volume confinement factor ($\sim 10^6$) compared with propagating mode. Meanwhile, both cavity and dipole mode can be effectively controlled through optical method. The numerical simulations quantitatively agree well with experimental results. This work will stimulate more theoretical study on localized graphene plasmons and open the way to build graphene nano-resonator, which is important for the future quantum devices and nano-manipulation of photons.

2. Nano-infrared imaging of propagating and localized graphene plasmons

Using s-SNOM system, we conduct the near-field optical measurements of graphene stripe with incident frequencies from 901 cm^{-1} to 980 cm^{-1}. The s-SNOM is based on an AFM (atomic force microscopy) operating in the tapping mode with $\Omega \sim 280$ kHz and an amplitude of ~ 30 nm. The metallic AFM tip confines the incident electric field into nanoscale and compensate the momentum mismatch between plasmons and free-space photons. The near-field signal is demodulated at a 4th harmonic in order to suppress background scattering. We normalize measured signal with Si reference sample as: $s_4(\omega) = s_4^0(\omega)/s_4^{\mathrm{Si}}(\omega)$. Here, $s_4^{\mathrm{Si}}(\omega)$ and $s_4^0(\omega)$ are the 4th demodulated near-field amplitude detected for Si standard reference sample and graphene, respectively. The graphene stripe is mechanically exfoliated from bulk graphite and transferred to 285-nm-thick SiO_2/Si substrate. The optical microscopy, AFM, and Raman spectrum are used to pick up single-layer graphene stripe structure without defects.

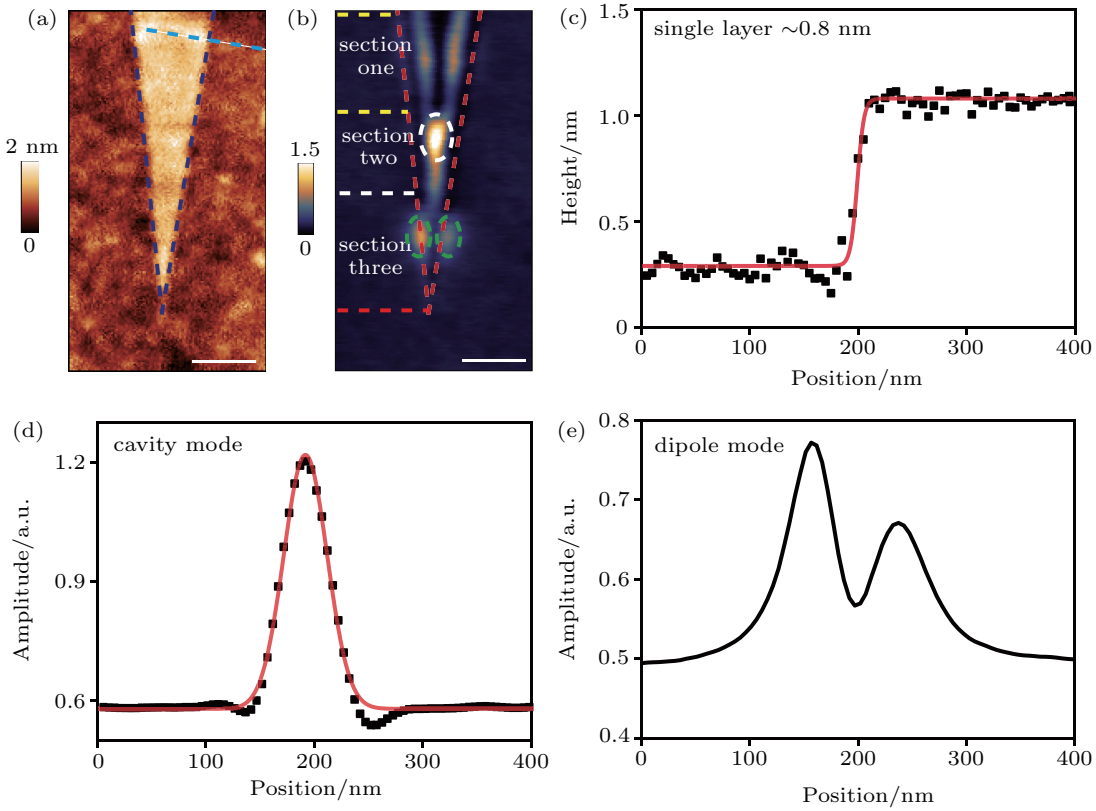


Fig. 1. (color online) Real-space optical imaging of graphene stripe. (a) AFM topography image of mechanically exfoliated graphene stripe. The darker area corresponds to the SiO_2/Si substrate. The outline of graphene is marked by blue dashed lines. (b) The corresponding nano-infrared optical image of graphene stripe with incident frequency of 930 cm^{-1}. The outline of graphene is marked by red dashed lines. The cavity mode and dipole mode are marked by white and green dashed circles, respectively. The scale bar is 200 nm. (c) AFM line-profile obtained from the cyan dashed line in panel (a). The experimental topography data (black squares) agrees well with Boltzmann fitting method. (d) Plasmonic line profile of cavity mode shown in panel (b). The experimental result (black squares) is well fitted by Gaussian shape. (e) Plasmonic line profile of dipole mode shown in panel (b).

In Fig. 1, we show the representative nano-infrared image of propagating and localized plasmons in graphene stripe. The AFM topography map (Fig. 1(a)) shows smooth graphene surface without wrinkles and defects. Figure 1(c) shows corresponding AFM line-profile along the cyan-dashed line in Fig. 1(a) and indicates that the height of monolayer graphene is ~ 0.8 nm. The near-field optical image (Fig. 1(b)) is collected at a selected IR frequency of 930 cm^{-1}, which can excite the graphene plasmons on SiO_2/Si substrate.[29] Due to the continuously changing width from ~ 400 nm to ~ 20 nm, there is an *in-situ* transition from propagating mode to localized mode in our graphene stripe. When the width of graphene

(W_{Gra}) is much larger than plasmonic wavelength (λ_p), it is expected to observe the propagating plasmons, whose most distinct hallmark is the presence of fringes parallel to the edge direction (Section one in Fig. 1(b)). The launched propagating wave spread radially outward from the AFM tip, reflect back upon reaching the graphene edge and finally form interference waves. Due to this method-intrinsic interference, we can extract the plasmonic wavelength through stretching twofold FWHM (full width at half maximum) of the dominated plasmonic fringes (Fig. S1).[30] When the W_{Gra} is similar to the plasmonic wavelength (Section two in Fig. 1(b)), graphene plasmons will produce cavity resonance in the nanoresonator. If the W_{Gra} continuously decreases and is much smaller than the wavelength (Section three in Fig. 1(b)), the localized dipole mode occurs. The physical mechanism is given in the Simulation parts in this manuscript. The corresponding line profiles of cavity mode and dipole mode are shown in Figs. 1(d) and 1(e), respectively. In Fig. 1(d), the near-field amplitude of cavity mode ($s_4(\omega) \sim 1.2$) is twice stronger than the conventional propagating mode ($s_4(\omega) \sim 0.5$). The previous calculation[9] indicates that the out-of-plane confinement of the graphene plasmon electric field is ~ 20 nm (Z_{local}). We define the three-dimensional volume confinement factor as the ratio between modal volume of free-space light (λ_0^3) and optical field volume of plasmons ($S_{local} \times Z_{local}$). Here, the S_{local} is the in-plane area of localized plasmons. From Fig. 1(b), we extract the S_{local} for cavity mode (white-dashed circle) and dipole mode (green-dashed circle) are 2.5×10^4 nm^2 and 1.4×10^4 nm^2, respectively. Hence, the volume confinement factor of cavity mode and dipole mode are 2.5×10^6 and 4.4×10^6, respectively. The experimental results show that the localized modes possess strong light–matter interaction and three-dimensional confining capability, which is inaccessible for propagating plasmons (just two-dimensional confinement).

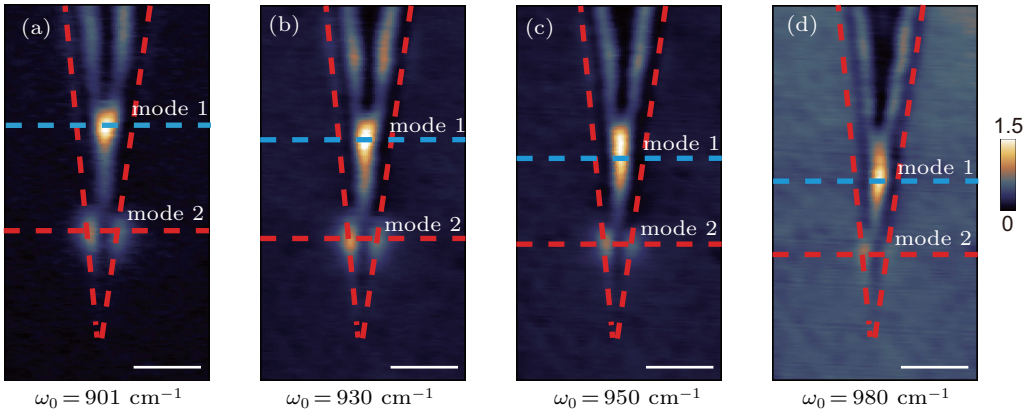


Fig. 2. (color online) The cavity mode and localized-dipole mode of graphene plasmons with different incident frequencies. (a)–(d) The near-field amplitude of graphene plasmons with incident frequency of 901 cm^{-1}, 930 cm^{-1}, 950 cm^{-1}, 980 cm^{-1}, respectively. Here, mode 1 and mode 2 represent cavity and dipole mode, respectively. The scale bar is 200 nm.

Based on theoretical prediction,[28,29] the propagating graphene plasmons show dispersive behavior and their wavelengths decrease when the incident frequencies increase. Figure 2 shows the variation trend of both propagating and localized modes when we change the incident frequency. Due to the interaction between graphene plasmons and optical phonon from SiO_2 substrate, the plasmonic amplitude becomes lower when the incident frequency change to 980 cm^{-1} (Fig. 2(d)). As shown in Fig. S1, the plasmonic wavelength decreases from 114.6 nm to 93.2 nm when the incident frequency increases from 901 cm^{-1} to 980 cm^{-1}. This phenomenon can be easily explained by dispersion relation of graphene plasmons. It is worth noting that the resonant widths of cavity and dipole mode decrease when the incident frequency increases, as shown by cyan and red dashed lines in Fig. 2. The resonant widths of graphene stripe for cavity mode of plasmons are 142.0 nm (Fig. 2(a)), 119.7 nm (Fig. 2(b)), 107.7 nm (Fig. 2(c)), 102.0 nm (Fig. 2(d)), respectively, when the incident frequencies are 901 cm^{-1}, 930 cm^{-1}, 950 cm^{-1}, 980 cm^{-1}. Under the same incident frequency, the resonant widths for dipole mode are 65.1 nm, 58.2 nm, 52.6 nm, and 43.0 nm. The resonant width of graphene plasmons is proportional to its wavelength.[28] As shown in Fig. S4, we extract the resonant condition as $W_{Gra}/\lambda_p \sim 1.17$ for cavity mode and $W_{Gra}/\lambda_p \sim 0.56$ for dipole mode. The phenomenon in Fig. 2 indicates that the cavity and dipole mode of graphene plasmons are both easily tunable through optical method (incident illumination), which is important for the future subwavelength applications.

3. Simulation results and discussion

In order to study the physical mechanism of cavity resonance and dipole mode, we conduct the numerical simulations by the finite element method (FEM) using commercial software package COMSOL in a wave optics module. When the width of graphene decreases to a similar value of the plasmonic wavelength ($W_{Gra} \approx \lambda_p \sim 100$ nm), the propagating

wave produces interference and resonant cavity mode. In order to launch the graphene plasmons, we set a vertically oriented electric point dipole 30 nm above graphene sample (inset in Fig. 3(a)), which is similar to the distance between tip and sample in the experimental measurement. In the model, graphene is set as a surface current layer with $J = \sigma E$, where σ is the local conductivity of graphene. The σ is given by Random phase approximation (RPA) as follows:[28,29]

$$\sigma(q \to 0, \omega) = \frac{e^2 E_F}{\pi\hbar^2} \frac{\mathrm{i}}{\omega + \mathrm{i}\tau^{-1}} + \frac{e^2}{4\hbar}\left[\theta(\hbar\omega - 2E_F) + \frac{\mathrm{i}}{\pi}\log\left(\left|\frac{\hbar\omega - 2E_F}{\hbar\omega + 2E_F}\right|\right)\right]. \quad (1)$$

Here, ω is the incident frequency and E_F is the absolute value of Fermi level of graphene. The $\hbar$ is reduced Planck Constant. The first and second terms of Eq. (1) describe the conductivity for the intraband and interband process, respectively. The maximum excitation photon energy in our experiments is ~ 0.12 eV, which is much smaller than interband transition energy ($2E_F \sim 0.4$ eV). Hence, we neglect the interband transition and simplify the conductivity with Drude approximation,

$$\sigma = \frac{e^2 E_F}{\pi\hbar^2} \frac{\mathrm{i}}{\omega + \mathrm{i}\tau^{-1}}. \quad (2)$$

In the simulation, we set the Fermi level as 0.2 eV, which is experimentally extracted from Raman measurements (Fig. S2). We record the normalized $|E|$ (absolute value of electric field) inside the graphene resonator. In Fig. 3(a), we show the representative simulation of near-field amplitude under the incident frequency of 930 cm^{-1}. It is observed that the plasmonic amplitude in the resonator center (purple area in Fig. 3(a)) changes when we control the widths of graphene. The resonant width for $\omega_0 = 930$ cm^{-1} is about 120 nm, with maximum amplitude. In Fig. 3(b), we summarize the calculated central near-field intensity under different incident frequencies and graphene widths, shown as background color. It is observed that the resonant W_{Gra} has a decreasing trend when the incident frequency increase from 900 cm^{-1} to 980 cm^{-1}. The corresponding widths are 130 nm±10 nm and 100 nm±8 nm for the incident wavenumber of 901 cm^{-1} and 980 cm^{-1}, respectively. The discrete points show the extracted experimental resonant widths of graphene from Fig. 2. The agreement between numerical simulation and near-field measurement indicate that we observe the cavity resonance of propagating graphene plasmons.

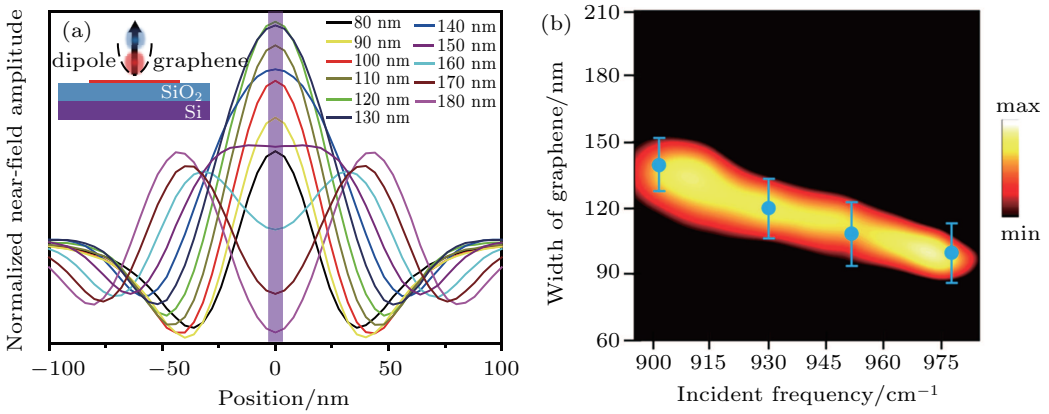


Fig. 3. (color online) Corresponding width of graphene for cavity resonance mode. (a) The calculated near-field amplitude in graphene resonator with different widths under the incident frequency of 930 cm^{-1}. The schematic of simulation model is shown in inset. We record the amplitude in the center of graphene (shown as purple area). (b) Numerically simulated amplitude in the graphene center for different widths and incident frequencies (background color). The discrete dots show the experimental W_{Gra} for cavity modes extracted from Fig. 2. The consistency between experimental results and numerical simulations indicate that we observe and control the cavity mode of graphene plasmons.

When we further decrease the width of graphene ($W_{Gra} \ll \lambda_p$), the localized mode of graphene plasmons is excited. Similar to metallic plasmonics, scattering spectrum is the most powerful tool to characterize the optical property of localized plasmons, including dipole, quadrupole, and even other multipole modes. In order to simulate the scattering cross section, we calculate the energy dissipation of external electric field around graphene nanoribbon. The scattering cross section can be expressed by[31]

$$\sigma_{Sca} = \frac{1}{I_0} \iint \boldsymbol{n} \cdot \boldsymbol{P} \mathrm{d}S,$$

where $\boldsymbol{n}$ is the normal vector pointing out to the graphene surface, $\boldsymbol{P}$ is the Poynting vector, and I_0 is input intensity. In Fig. 4, the dashed lines show calculated scattering spectrum of graphene with incident frequencies of 901 cm^{-1} (black), 930 cm^{-1} (red), 950 cm^{-1} (green), and 980 cm^{-1} (blue), respectively. All scattering spectra show an individual dipolar resonance peak when the W_{Gra} change from 20 nm to 160 nm. Experimentally, we extract the W_{Gra} for dipole mode from Fig. 2, which is shown in Fig. 4 as solid lines. The agreement between calculated spectra and experimental results with all incident frequencies indicates that we actually observe the localized dipole mode of graphene plasmons.

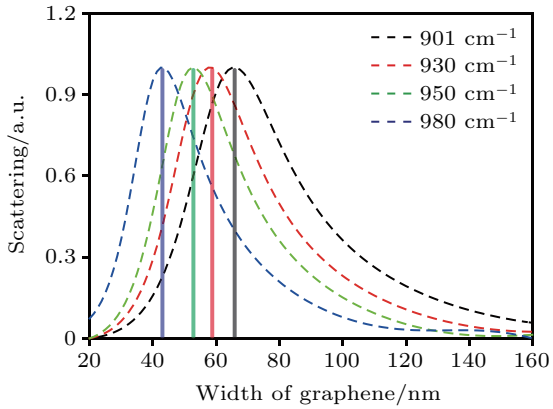


Fig. 4. (color online) Calculated scattering spectrum of graphene. The dashed lines represent calculated spectrum with incident frequencies of 901 cm^{-1} (black), 930 cm^{-1} (red), 950 cm^{-1} (green), and 980 cm^{-1} (blue), respectively. The solid lines are experimental W_{Gra} for dipole modes extracted from Fig. 2.

4. Conclusions

In this manuscript, we conduct the in-situ nano-infrared imaging of plasmonic transition from propagating, cavity mode and finally localized dipole mode in graphene stripe with continuously changing width. When the width of graphene is similar with plasmonic wavelength ($W_{\mathrm{Gra}} \approx \lambda_{\mathrm{p}} \sim 100$ nm), we observe the cavity resonant phenomenon, with enhanced near-field amplitude ($\sim$ twofold) and high-volume confining ability ($\sim 2.5 \times 10^6$). The localized dipole mode is excited if the width further decreases much smaller than the wavelength ($W_{\mathrm{Gra}} \ll \lambda_{\mathrm{p}}$). Both cavity mode and dipole mode can be effectively tuned through optical method. The numerical simulations agree well with experimental measurements. Our findings represent an efficient tool for studying the localized graphene plasmons and stimulate further theoretical work of localization in polaritonics field.

References

[1] Barnes W L, Dereux A and Ebbesen T W 2003 *Nature* **424** 824
[2] Rotenberg N and Kuipers L 2014 *Nat. Photon.* **8** 919
[3] Basov D N, Fogler M M and De Abajo F J G 2016 *Science* **354** 6309
[4] Low T, Chaves A, Caldwell J D, Kumar A, Fang N X, Avouris P, Heinz T F, Guinea F, Martin-Moreno L and Koppens F 2017 *Nat. Mater.* **16** 182
[5] Gramotnev D K and Bozhevolnyi S I 2010 *Nat. Photon.* **4** 83
[6] Schuller J A, Barnard E S, Cai W, Jun Y C, White J S and Brongersma M L 2010 *Nat. Mater.* **9** 193
[7] Dai S Y, Fei Z, Ma Q, Rodin A, Wagner M, McLeod A, Liu M, Gannett W, Regan W and Watanabe K 2014 *Science* **343** 1125
[8] Yoxall E, Schnell M, Nikitin A Y, Txoperena O, Woessner A, Lundeberg M B, Casanova F, Hueso L E, Koppens F H and Hillenbrand R 2015 *Nat. Photon.* **9** 674
[9] Woessner A, Lundeberg M B, Gao Y, Principi A, Alonso-González P, Carrega M, Watanabe K, Taniguchi T, Vignale G and Polini M 2015 *Nat. Mater.* **14** 421
[10] Nie S and Emory S R 1997 *Science* **275** 1102
[11] Kneipp K, Wang Y, Kneipp H, Perelman L T, Itzkan I, Dasari R R and Feld M S 1997 *Phys. Rev. Lett.* **78** 1667
[12] Engheta N 2007 *Science* **317** 1698
[13] Fang Y, Li Z, Huang Y, Zhang S, Nordlander P, Halas N J and Xu H 2010 *Nano Lett.* **10** 1950
[14] Atwater H A and Polman A 2010 *Nat. Mater.* **9** 205
[15] Gramotnev D K and Bozhevolnyi S I 2014 *Nat. Photon.* **8** 13
[16] Schnell M, Alonso-Gonzalez P, Arzubiaga L, Casanova F, Hueso L E, Chuvilin A and Hillenbrand R 2011 *Nat. Photon.* **5** 283
[17] Khurgin J B 2015 *Nat. Nanotechnology* **10** 2
[18] Geim A K and Grigorieva I V 2013 *Nature* **499** 419
[19] Low T and Avouris P 2014 *ACS Nano* **8** 1086
[20] Geim A K and Novoselov K S 2007 *Nat. Mater.* **6** 183
[21] Nair R R, Blake P, Grigorenko A N, Novoselov K S, Booth T J, Stauber T, Peres N M and Geim A K 2008 *Science* **320** 1308
[22] Li Z, Henriksen E A, Jiang Z, Hao Z, Martin M C, Kim P, Stormer H, Basov D N and 2008 *Nat. Phys.* **4** 532
[23] Ju L, Geng B, Horng J, Girit C, Martin M, Hao Z, Bechtel H A, Liang X, Zettl A and Shen Y R 2011 *Nat. Nanotechnology* **6** 630
[24] Yan H, Low T, Zhu W, Wu Y, Freitag M, Li X, Guinea F, Avouris P and Xia F 2013 *Nat. Photon.* **7** 394
[25] Ni G, Wang L, Goldflam M, Wagner M, Fei Z, McLeod A, Liu M, Keilmann F, Özyilmaz B and Neto A C 2016 *Nat. Photon.* **10** 244
[26] Efetov D K and Kim P 2010 *Phys. Rev. Lett.* **105** 256805
[27] Wang L, Meric I, Huang P, Gao Q, Gao Y, Tran H, Taniguchi T, Watanabe K, Campos L and Muller D 2013 *Science* **342** 614
[28] Chen J N, Badioli M, Alonso-González P, Thongrattanasiri S, Huth F, Osmond J, Spasenović M, Centeno A, Pesquera A and Godignon P 2012 *Nature* **487** 77
[29] Fei Z, Rodin A, Andreev G, Bao W, McLeod A, Wagner M, Zhang L, Zhao Z, Thiemens M and Dominguez G 2012 *Nature* **487** 82
[30] Ni G, Wang H, Wu J S, Fei Z, Goldflam M D, Keilmann F, Ozyilmaz B, Neto A H C, Xie X and Fogler M M 2015 *Nat. Mater.* **14** 1217
[31] Bai Q, Perrin M, Sauvan C, Hugonin J and Lalanne P 2013 *Opt. Express* **21** 27371